Chinese Journal of Aeronautics, (2013),26(5): 1125–1134

Chinese Society of Aeronautics and Astronautics
& Beihang University

Chinese Journal of Aeronautics

cja@buaa.edu.cn
www.sciencedirect.com

Using a pressure controlled vortex design method to control secondary flow losses in a turbine stage

Deng Qingfeng [a,b], Zheng Qun [a,*], Yue Guoqiang [a], Zhang Hai [a], Luo Mingcong [a]

[a] *College of Power and Energy Engineering, Harbin Engineering University, Harbin 150001, China*
[b] *No. 703 Research Institute, China Shipbuilding Industry Corporation, Harbin 150078, China*

Received 9 July 2012; revised 16 September 2012; accepted 20 November 2012
Available online 5 September 2013

KEYWORDS

Pressure control;
Pressure controlled vortex design;
Secondary vortex;
Stream surface variation;
Turbine design

Abstract A turbine design method based on pressure controlled vortex design (PCVD) is presented to design a small-size turbine stage. Contrary to the conventional controlled vortex design (CVD) method, the main objective of PCVD is to control the axial velocity and radial pressure in the stator–rotor gap. Through controlling axial velocity, the PCVD establishes a direct tie to meridional stream surface. Thus stream surface variation is induced, resulting in a large secondary flow vortex covering the full blade passage in the respective stator and rotor. This secondary flow vortex could be dedicated to control the secondary flow mitigation and migration. Through radial pressure, the PCVD is also associated with the macroscopic driving force of fluid motion. So the better benefit of CVD can be achieved. The core concept behind PCVD is to mainly control the spanwise pressure gradient by altering profile loading at various spanwise locations. Therefore not only the local profile lift is affected, but also the resulting throat widths, stage reaction degree, and massflow rate are altered or redistributed respectively. With the PCVD method, the global stage efficiency is increased successfully while the mass flow rate keeps constant. Additionally there is no endwall shape optimization, stacking optimization, or pitch/chord variations, concentrating solely on varying blade profile deflections and stagger.

1. Introduction

Both blade design and optimization continue to be explored to meet the ever-increasing gas or steam turbine performance demands. Thus more attentions are drawn to the blade design for higher-efficiency turbines.

The fundamental problem in designing efficient and high-performance turbine stages is large flow losses in the endwall regions, particularly at the root in a low-reaction turbine. The poor performance generally resulting from the boundary layer fluid separation in the endwall regions results in large local flow losses and blockage of fluid which forces the mainstream to flow towards the mid-span. A few decades ago, a controlled vortex design (CVD) system was proposed which essentially increased blade circulation along the dominant part of blade span. Since the first publication of the CVD method

* Corresponding author. Tel.: +86 451 82518116.
E-mail address: zhengqun@hrbeu.edu.cn (Q. Zheng).

Peer review under responsibility of Editorial Committee of CJA.

ELSEVIER Production and hosting by Elsevier

1000-9361 © 2013 Production and hosting by Elsevier Ltd. on behalf of CSAA & BUAA. Open access under CC BY-NC-ND license.
http://dx.doi.org/10.1016/j.cja.2013.04.028

regard to turbine design by Dorman et al.,[1] a considerable amount of research[2–9] has been done after that. It is well known that the CVD method possesses the potential to decrease secondary flow losses. However, up till now the CVD effects on a turbomachinery flow field are of uncertainty. Most of studies have still been conducted through academic research which is based on particular machines or blades. In other words, there appears no consensus on secondary flow control mechanisms about CVD. First contribution to the preliminary understanding of CVD's impact on secondary flow behaviors was made by Friedrichs et al.[10] and Gümmer et al.[11] at the beginning of the 21st century. Actually this work is limited to investigate blade lean and sweep in turbines and compressors. The deliberate use of blade lean and sweep has attracted more and more interests during the last few years. Several researchers[12,13] had done a lot of work and relevant results are provided in their publications. While CVD is a well-worn topic, any innovation of this method and an improved understanding are prerequisites for further improvements in turbine efficiency. This leads to searching a new way to solve the problem mentioned, so the present pressure controlled vortex design (PCVD) system is born. The current method in this paper is developed from Ref.[14] and is an extension of early studies.

The present paper describes aerodynamic design and numerical result analysis of a single-stage turbine. Particular emphasis is put on PCVD application and verification in blade design. Furthermore, efforts are made to find the intrinsic relations between geometric and aerodynamic parameters.

2. Design methodology

2.1. PCVD process

The flow chart of the PCVD method is shown in Fig. 1. Prior to PCVD, a one-dimensional (1D) preliminary design process is used to estimate annulus shape, stage number, blade number, aspect ratio, mean-line velocity triangles, and blade loading levels in each stage. Then PCVD follows, in which three-dimensional (3D) velocity diagrams at all radii except the mean radius are obtained by solving the radial equilibrium equation. These velocity diagrams are chosen based on good choices of axial velocity and radial pressure distributions. Once the 3D velocity diagrams are obtained, the blade profiles can be easily parameterized through a number of parameters with several polynomials. Hence 3D turbine blades can be generated by stacking the two-dimensional (2D) blade sections. After the blade design is completed, a viscous simulation is carried out to verify the 3D flow field and evaluate the turbine performance. If the design intents are not met, some new changes have to be made to the blade shape based on the results of last changes.

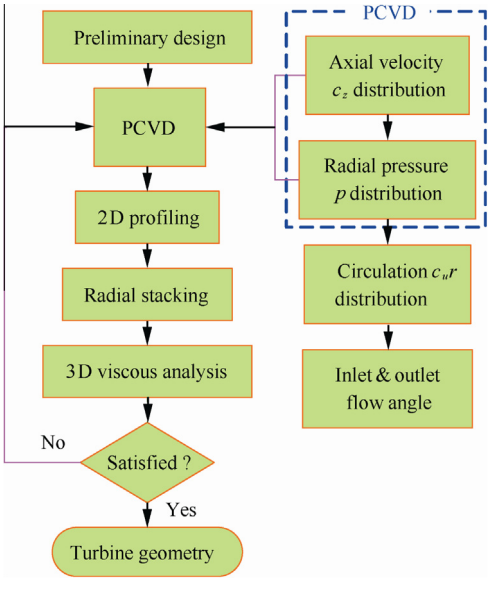

Fig. 1 Flow chart of the PCVD method.

Changing the radial pressure gradient is an efficient way to prevent secondary flow losses during the turbine blade design process, since the 3D flow field is largely driven by the pressure. That is to say the PCVD system has advantages of the pressure-control approach besides features of the CVD technique. The main drawback of PCVD is that the method relies on the user's experience to select a proper axial velocity distribution between the stator and the rotor.

The baseline turbine is derived from a 1.5-stage test facility which is operated in a subsonic flow condition. The turbine stage consists of 30 stator blades and 45 rotor blades. All the blade rows have an outside diameter of 500 mm and a hub diameter of 340 mm. The running tip clearance is 0.4 mm (0.5% of the blade span). At the design rotating speed of 7000 r/min, the inlet Reynolds number and the Mach number are 4.28×10^5 and 0.19, respectively. This turbine stage is designed with a free vortex design (FVD) method. An advanced aft-loaded blade is incorporated into the stator design to further reduce flow losses and increase turbine efficiency.

2.2. Axial velocity decision

With increase of the blade diameter-to-height ratio to some degree, the exit axial velocity behind the stator can be considered as a uniform distribution in a sense. Since modern turbines are designed to achieve light, compact, and highly efficient systems, this ideal state dose not exist. The flows through modern turbines are more complex due to fact that the blade diameter-to-height ratio is very low, about 2.625 for the present case, so the inner part of blades operates in a high subsonic or even transonic condition. It means the reaction degree at the turbine stage root is excessively low and the rotor blade deflection angle is very large. For above reasons, it is desirable to adjust the blade design at radial stations in order to relieve root flow conditions and fully develop work capacity done by blades.

PCVD is very similar to the conventional CVD. All the radial flow distributions in both methods are specified and tailored to maximize individual stage efficiency. Yet, contrary to the conventional CVD method with a direct assumption of circulation distribution, the main objective of PCVD is to control the axial velocity in the stator–rotor gap. Then the question becomes how to decide the axial velocity distribution. A simple strategy is to modify the prototype flow pattern (a constant massflow pattern is adopted in FVD turbine stage), so there is a smaller or larger axial velocity leaving the stator. A detailed description about this approximate engineering method is presented in Ref.[14] As illustrated in Fig. 2, the radial massflow distribution between the stator and the rotor inclines distinctly to a peak near the hub, which is the design intent to

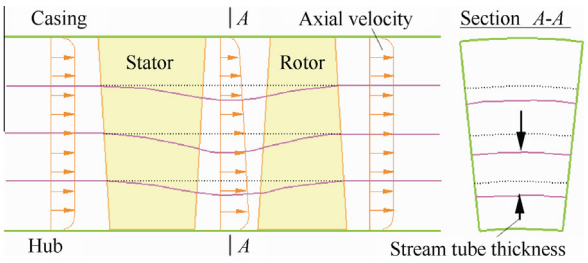

Fig. 2 PCVD effect on stream surfaces.

unload the stator hub and energize the rotor boundary layer momentum. Simultaneously, the change of radial massflow at the stator exit near the hub must be compensated by a change near the tip according to the conservation of fluid mass at the prescribed design flow rate. Such an aerodynamic arrangement tends to make the stator exit flow non-uniform with a high axial velocity near the hub and a low velocity near the tip. In addition, the axial velocity at the stator exit decreases with increasing radius while the tangential velocity increases with radius, thus reducing the relative inflow velocity to the rotating blade.

The streamlines are relevant to axial velocity variation and the axial velocity variation causes the streamlines on the meridional plane to move towards the hub. The meridional streamline curvature, spanwise pressure gradient, and blade loading are altered accordingly. We can infer that the streamline curvature is proportional to the axial velocity variation and the magnitude of radial static pressure change is also mainly dependent on this variation. As depicted in Fig. 2, the meridional stream surfaces are affected and the cylindrical stream surfaces do not exist. The stream surface thickness, which is more easily considered as the perpendicular distance between two adjacent axisymmetric stream surfaces, is also affected. Those deviations of stream surfaces are already predictable in the full 3D calculation.

The axial velocity variation often involves opening the stator blade throat near the hub endwall and closing it in the tip region. During the design process, not only the exit flow angle but also the stagger angle is modified to deliver an intended radial massflow distribution. The radial distributions of FVD and PCVD stator exit flow and stagger angles are shown in Fig. 3. A comparison is made between PCVD and FVD. Unless otherwise specified, all the flow angles referred in this paper are measured in the tangential direction. Additionally, the stagger angle is defined as the angle between the chord line and the turbine axial direction. As indicated in Fig. 3, the stator exit flow angle decreases with increasing radius while the stator stagger angle increases with radius. The rotor exit flow and stagger angles, which are not presented here, are altered as little as possible from the FVD stage.

2.3. Pressure control instead of circulation control

As mentioned earlier, the spanwise static pressure redistribution is caused as well by tuning the axial velocity distribution in the stator–rotor gap. Hence a pressure control concept is proposed instead of circulation control which is commonly used in conventional CVD. Fig. 4 shows the typical radial pressure distributions at the stator exit before and after PCVD. In this study, a linear distribution of radial pressure in the inter-row gap is obtained from radial equilibrium equations. It can be seen that PCVD leads to a flat tendency of static pressure distribution in the stator–rotor gap. Thus a more even loading across the stator blade height is produced due to PCVD. A main benefit of PCVD can be arisen from the uniform pressure field provided to the downstream rotor. Meanwhile, the radial static pressure in the stator–rotor gap represents the stage reaction distribution, supposing the stage inlet and outlet conditions are fixed. Once the axial velocity and static pressure distributions are determined, the inter-row circulation distribution could be resolved immediately to aid blade design.

There are several reasons why pressure control has advantages over circulation control. Firstly, relative to the circulation law, the deviations from radial pressure distribution between initial and final designs are minimal due to its pressure magnitude. Secondly, the radial equilibrium inside a turbine stage can also be easily satisfied with pressure distribution. Thirdly, the radial pressure distribution in the inter-row gap can be approximated as a simple curve (e.g., a linear curve in this study) while the circulation would be a high-order polynomial. Particularly, the radial pressure distribution in a real turbine is roughly known, so the rationality and validity of pressure distribution could be inspected in advance. Although a number of papers have been written to centre on

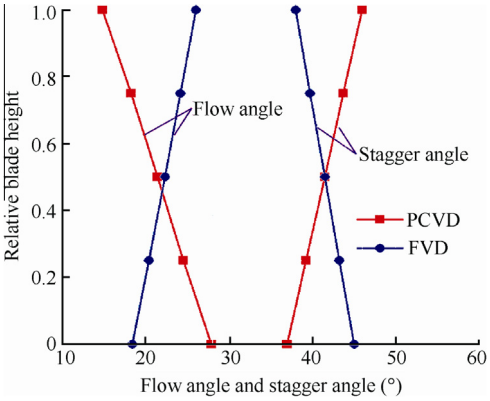

Fig. 3 Radial distributions of FVD and PCVD stator exit flow and stagger angles.

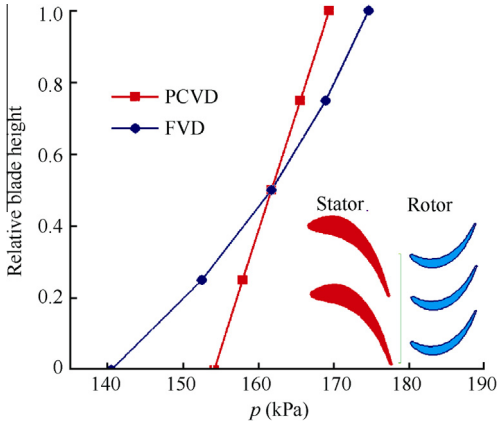

Fig. 4 Sketches of radial pressure distributions at the stator exit.

conventional CVD, the models of circulation distributions are various and only valid for certain configurations in most cases. While in PCVD, the final pressure distribution is assumed to be a harmonious state with a uniform pressure field across the rotor–stator gap.

2.4. Stream surface variation and secondary flow control mechanism

The basic flow mechanisms related to PCVD in a turbine stage and the internal relations between PCVD and flow behaviors are described and illustrated in Fig. 5. As depicted in Fig. 5(a), a streamline offset induced by PCVD begins at the stator leading edge (LE) and ends at the rotor trailing edge (TE). This has changed the streamline flow patterns in such a way that the suction surface (SS) streamlines are deflected towards the hub and the pressure surface (PS) streamlines are diverted towards the casing. All of these attributes above can fully reflect the "stage" design intent of PCVD. The streamlines in Fig. 5(a) also represent the stream surface twist and deflection.

Corresponding sketches of shear stress lines on PCVD blade surfaces with realistic stream surfaces are presented in Fig. 5(b). The classical and PCVD-induced secondary flow vortexes are also shown in this figure. The twisted stream-surface at mid-height creates a large secondary flow vortex covering the full blade passage in respective stator and rotor. The PCVD-induced passage vortex is counteractive to the classical cross-passage flow in the hub and supports the cross-passage flow in the casing. Therefore, the secondary flow pattern has a much higher level of complexity in PCVD than in conventional design methods. The new PCVD-induced secondary vortex, which rotates opposite to the classical passage vortex, prevents the hub endwall low-momentum fluid from interacting with the SS boundary layer. A very compact passage vortex is resulted from the considerably-reduced boundary layer interaction. The radial migration on the blade surface is also deflected when striking the new vortex. The PCVD-induced secondary vortex, which has the same rotating direction as the classical passage vortex, promotes the secondary flow from PS to SS. The transverse boundary layer near the tip is expanded and leaves the casing, restraining near-tip accumulation of high-loss fluid. The loss-modification effects of PCVD are rather analogous to the functions in sweep/skew as described in Refs.[10,11] Although the radial migration deflection on the blade surface is clearly visible and verified in the analysis part of this paper, the PCVD-induced secondary vortex could not be captured using a CFD approach or experiment at present.

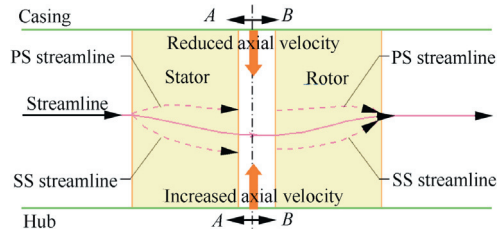

(a) PCVD effect on streamlines

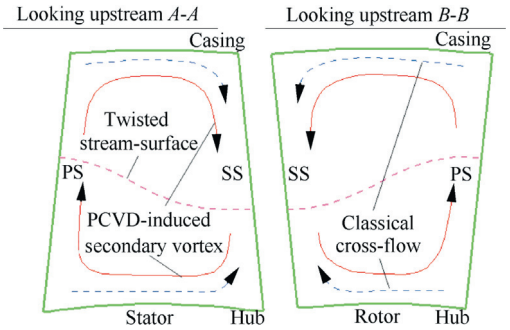

(b) PCVD effect on secondary components

Fig. 5 Secondary flow loss control mechanism of PCVD.

3. Parametric design

ANSYS has developed a unique tool for blade cross section design. In this tool, called Blade Geometry, blade cross section shapes are expressed through the Bézier polynomial curves. The Bézier curves can accurately represent an arbitrary shape with relatively less geometric control points. Hence, only a small number of design variables are needed in the design procedure. Through a user-friendly graphical interface, an aerodynamic designer can directly control over a series of familiar geometry parameters such as blade stagger, passage throat, blade thickness, cross section area, and LE and TE wedge angles.

The blade shape design has the following contents: (1) cross section design at different blade heights by giving inlet and outlet flow angles, stagger angles, blade thickness distributions, etc.; (2) radial stacking of all blade cross sections. In this study, five sections at 0%, 25%, 50%, 75%, and 100% span stations are chosen for each blade row.

3D views of FVD and PCVD blade geometries are shown in Fig. 6. The PCVD stator is closer to the adjacent blade at the tip and more open at the hub, featuring strong tangential lean around the TE at the mid-section. Hence the stator PS faces the hub. As a consequence of a change to the absolute flow angle distribution at the stator outlet, the relative flow angle distribution at the rotor inlet is also modified, so the rotor becomes less skewed with a very low inlet flow angle at the tip. In addition, the FVD results in an extremely twisted rotor that is difficult for mechanical design.

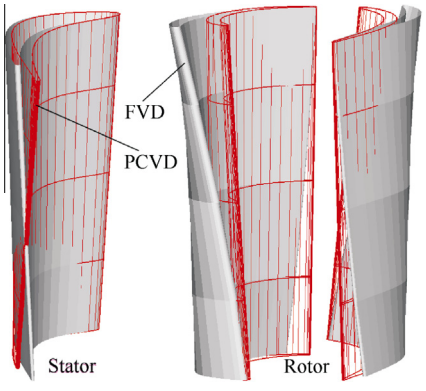

Fig. 6 Geometry comparison of FVD and PCVD blades.

4. Computation methodology

To validate PCVD effects on turbine performance, a 3D viscous numerical simulation is conducted.

4.1. Solver

Numerical simulations are run using EURANUS, a CFD code developed by NUMECA. The code is based on a finite difference scheme to solve the Reynolds averaged Navier–Stokes equations in conservative formulation. In this scheme, the Navier–Stokes equations are discretized with a cell-centered finite volume algorithm in space and an explicit four-stage Runge–Kutta method in time. For turbulence closure, a Spalart–Allmaras model is adopted, which is theoretically robust in numerical calculations and has numerical accuracy for boundary layer turbulent flow calculations. The EURANUS solver convergence is accelerated by local time stepping, implicit residual smoothing, and multigrid acceleration techniques. In addition, the solver has been parallelized using a domain decomposition method and runs efficiently on a personal computer with a quad-core processor.

4.2. Computation grid

The AutoGrid module in NUMECA is used to generate computational meshes. Both transfinite interpolation method and elliptic grid generation system are used to generate hybrid O–H meshes. The complete numerical domain of the turbine stage is shown in Fig. 7. A multi-block structure grid of 943146 nodes is adopted to discretize the computational domain. The H-type grids are used for inlet and outlet blocks, while the composite O/H-type grids are utilized for passage blocks in order to reduce the grid skewness and facilitate solving the boundary layer around the blades. The tip clearance gap is also modeled and the relative motion between the rotor and the casing is included. The meshes are compressed next to the solid wall so as to achieve a y^+ value of 1 as the Spalart–Allmaras turbulence model requirement. A minimal skewness angle more than 12° is achieved through the hex mesh. A study of grid independence is conducted to confirm whether this grid is sufficient or not to reach an enough accurate solution. Detailed computation results are summarized in Table 1. The maximum deviation of performance characteristics among these computations for the PCVD turbine geometry is only 0.106%. Therefore we believe that the current computation grid is sufficient and further refinement is needless for numerical solution fidelity. A same mesh topology is selected to simulate the flows in PCVD and FVD turbine stages.

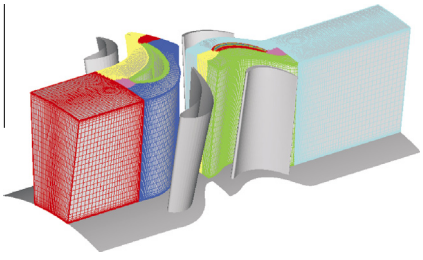

Fig. 7 Complete numerical domain of the turbine stage.

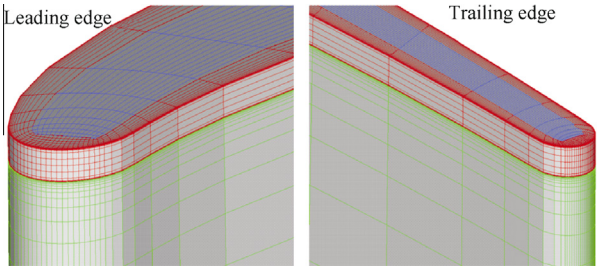

Fig. 8 Close-ups of mesh topology in the rotor tip clearance region around the LE and TE.

Fig. 8 shows the close-ups of mesh topology in the rotor tip clearance region around the LE and TE. AutoGrid models the gap in a consistent way that meshes the blade geometry. The tip clearance grid is made up of 2 blocks (O–H topology) and 13 layers are laid inside the clearance region. The meshes at the near-wall, endwall, LE, and TE of the rotor are refined. For a single-passage grid, such settings have a good resolution of LE, TE, and blade wake.

The baseline turbine boundary conditions are also derived from the 1.5-stage test facility. Same boundary conditions are employed for PCVD and FVD turbine stages. For each computation, the total temperature, total pressure, and flow direction are fixed at the inlet, while the average static pressure is imposed at the outlet. Periodic boundary conditions are used on the lateral faces of the whole flow domain. A conservative coupling by pitchwise row approach has been adopted at the interface between the stator and the rotor. All the solid walls are treated as adiabatic and no-slip. Finally, a nominal rotation speed of the test turbine is applied. A stable convergence of the CFD solver requires about 1000 iterations, which take about 2 h.

5. Results and discussions

To demonstrate the aerodynamic performance impact of the PCVD method, two distinct turbine stages have been numerically assessed with regard to section load and secondary flow generation.

5.1. Overall performance

As shown in Table 2, an overall efficiency gain of 0.95% has been achieved in the PCVD turbine stage relative to the

Table 1 Grid independence study of the PCVD turbine.

Grid number	9.43×10^5 nodes	1.23×10^6 nodes	1.63×10^6 nodes	Maximum deviation (%)
Massflow G (kg/s)	15.129	15.118	15.113	−0.10576
Efficiency η (%)	92.713	92.772	92.788	0.080895
Total pressure ratio π^*	0.68293	0.68295	0.68295	0.002929
Power P (kW)	585.53	585.49	585.42	−0.01879

Table 2 Comparisons of the design results.

Computational term	FVD	PCVD	Increment (%)
Massflow G (kg/s)	15.12	15.129	0.06
Efficiency η (%)	91.839	92.712	0.95
Total pressure ratio π^*	0.6815	0.68293	0.21
Power P (kW)	582.48	585.53	0.52
Torque M (N·m)	794.61	798.77	0.52
Thrust T (N)	1966.8	1954	−0.65

FVD turbine stage. Some comprehensive measures like reducing blade count, improving profile design, blade lean, and improving rotor tip seals are not included in the design process. The turbine stage isentropic efficiency is increased from 91.839% to 92.712% while the total pressure ratio and mass flow are maintained. Other performance parameters such as power and torque are also increased. Another intriguing finding is that the axial thrust of the PCVD turbine stage is decreased.

5.2. Detailed flow characteristics

5.2.1. Influences on blade surface pressure

Fig. 9 illustrates the blade shapes and the corresponding blade surface static pressure changes made by PCVD. The reasons for controlling the pressure gradient are evident. For the PCVD stator, the spanwise distributions of the loading area are altered moderately. The loading near the casing is increased and the loading near the hub decreased. It can be interpreted that the blade load near the hub shifts towards the tip. The unloading of the stator hub due to PCVD gives a means for reduction of the cross-passage pressure gradient, so the cross flow, endwall boundary layer separation, and relevant secondary flow losses are reduced accordingly. This can be achieved by decreasing flow turning at the hub. Referring to Fig. 9, the PCVD stator is formed by opening the throat at the hub. To keep the overall throat area unchanged, an opposite effect occurs near the casing. The blade section is slightly over cambered at the tip relative to the pitchline shape.

There are two reasons why the axial thrust decreases in PCVD. The first explanation is that the increased load near the tip is nearly equal to the reduced load near the hub, so the stator total work remains unchanged or even improves a little bit and the rotor axial thrust decreases. Another argument is based on the redistribution of working fluid. Although the blade load near the hub is decreased, the work done by the lower part of the stator blade is actually increased due to the working fluid redistribution. Both explanations are reasonable, but the latter is more acceptable.

Fig. 10 shows a comparison of chordwise static pressure distributions on blade surfaces between FVD and PCVD rotors. There is a considerable redistribution of static pressure. Since the hub pressure at the stator exit increases, the pressure loading required in the PCVD rotor inner section increases. The PS exhibits a significantly increased pressure and the SS pressure decreases somewhat in the rear part. Hence the circumferential pressure gradient, frequently called the "driving force of the secondary flow", is increased remarkably at the hub region (10% span). Since most of the pressure drop is executed in the stator tip section, the amount of work performed

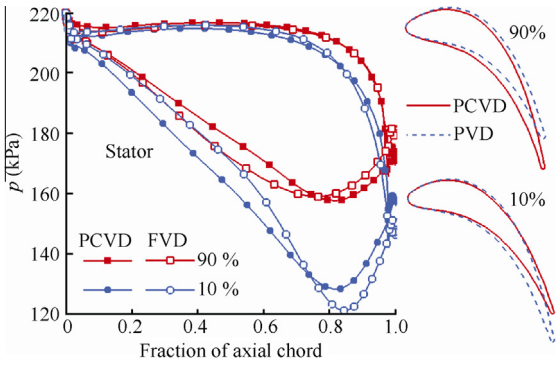

Fig. 9 Blade shapes and the corresponding blade surface static pressure changes made by PCVD.

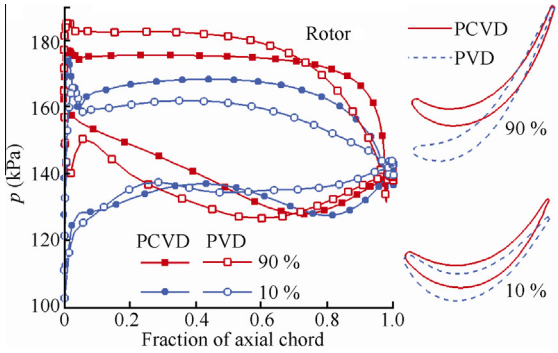

Fig. 10 Chordwise static pressure distribution on blade profile comparisons between FVD and PCVD rotors.

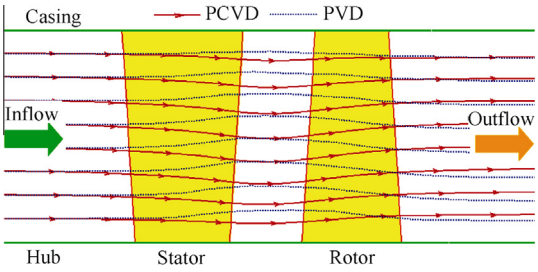

Fig. 11 Streamlines on the meridional plane.

by the PCVD rotor tip section is reduced. As we expect, the tip-section loading around the LE is decreased. Less secondary flow and tip leakage are initiated accordingly. Fig. 10 also presents the comparisons of the rotor hub and tip sections. The PCVD and FVD rotor blades use equivalent maximum thickness distributions. A mild twist rotor blade from hub to tip is obtained from PCVD. The chord length is maintained constant along the blade span to simplify blade manufacturing.

5.2.2. Influences on stream surfaces and reaction

The circumferentially mass-averaged streamlines on the meridional plane are shown in Fig. 11. In Fig. 11, the PCVD and FVD turbine meridional streamline distributions are superimposed on each other in order to compare those two turbine stages easily. The streamlines in PCVD divert to the hub

endwall in the front part of the stator and shift back to the rear part of the rotor. The greatest deflection angle of streamlines is near the mid-span. The resulted stream surface seems to be thicker near the casing and thinner near the hub. An opposite behavior is observed in the FVD turbine stage. The PCVD effects are almost confined in the turbine stage and have little influence on the upstream and downstream flow fields as evident in Fig. 11. The above results clearly support the assumptions made during the design process. The increased streamline curvature has been extensively used to increase the root reaction of low-pressure steam turbines as described by Stüer et al.[15] and Völker et al.[16] These machine root reactions are in very great danger of becoming negative.

The elemental annular blade cascade massflow is a really good indicator of stream surface thickness modification. We define the circumferentially averaged elemental annular blade cascade massflow Δm as the following:

$$\Delta m = 2\pi\rho r c_z \tag{1}$$

where ρ is the fluid density, r is the radius on the meridional plane, and c_z is the circumferentially averaged axial velocity.

The circumferentially averaged elemental annular blade cascade massflow distributions along the blade height are illustrated in Fig. 12(a), revealing the relative differences between

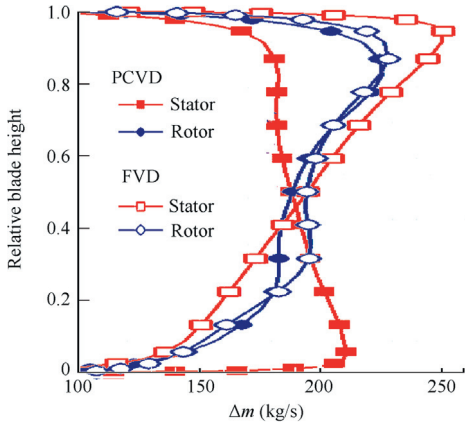

(a) Elemental annular blade cascade massflow distributions along the blade height

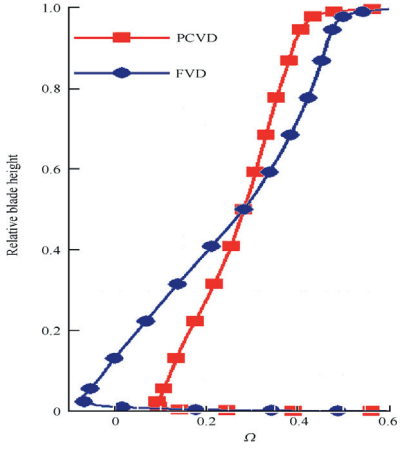

(b) Stage reaction distributions along the blade height

Fig. 12 Eemental annular blade cascade massflow and stage reaction distributions along the blade height.

PCVD and FVD. At the stator exit, a definite massflow increase is expected in the lower span region and a massflow deficit is observed near the casing. The reduced mass flow at the outer span can be deemed to move towards the hub region, so the total massflow cannot change much. This is what one expects. Behind the rotor blade, the PCVD rotor delivers the same radial massflow rate distribution as the FVD one. The elemental annular blade cascade massflow redistribution frequently brings about reaction change. Corroborating this argument, the stage reaction Ω distributions along the blade height is additionally illustrated in Fig. 12(b). There is considerable reaction redistribution and its spanwise gradient is decreased. Relative to FVD, the root reaction is increased in a certain degree to improve the root performance and the tip reaction is decreased to reduce the tip leakage. Note that the level of turbine stage reaction alterations in the upper part is nearly the same as in the lower part. It can be viewed as a symmetric effect around the middle height. This can be explained in terms of streamline curvatures induced by PCVD.

5.2.3. *Influences on flow loss and efficiency*

To identify loss reduction regions due to PCVD, the relative total pressure loss coefficients of blade rows and the turbine stage's isentropic efficiency along the channel height are evaluated in Fig. 13. The loss in the PCVD stator is simply redistributed. The PCVD stator loss at the root is considerably decreased due to the fact that the stator root is unloaded. However, this loss reduction near the hub is usually at the expense of increased loss at the stator tip. Obviously a trade-off exists between the increased profile loss and the reduced secondary flow loss in the PCVD stator. A key to a successful 3D design incorporating PCVD appears to achieve this correct balance. The most total pressure loss of the reference rotor comes from the passage vortex area near the endwalls. As depicted in Fig. 13, the relative total pressure loss of the PCVD rotor is substantially lower than that of the FVD rotor in the lower region between 12.5% and 60% span. This is a direct consequence of PCVD delivering higher massflow to the inefficient hub sections. A slightly lower loss is also obtained above 75% span. Directly at the rotor hub endwall, a negative loss is observed. It might be because the high-momentum fluid replaces the low-momentum boundary layer at the rotor inlet wall. The most significant result is indicated by a radial evaluation of the efficiency difference between PCVD and FVD stages. The maximum efficiency improvement is nearly 5.4 points at 36% span. Most of efficiency improvement is located between 18% and 60% of the blade span which causes a positive influence on overall stage efficiency.

No distinct loss reduction is observed in the PCVD stator. The net effect of PCVD seems only to improve the rotor performance. Especially PCVD guarantees a better utilization of rotor blade sections at lower radii. For above reasons, the following discussions will be focused on rotor flow characteristics.

5.2.4. *Influences on secondary flow*

Fig. 14 reports the limiting streamlines on rotor blade surfaces. In a sense, PCVD potential effect can be identified when comparing the PS and SS streamline differences of PCVD and FVD turbine stages. Inspecting the upper and lower figures, PCVD leads to a weaker rollup of the passage vortex separa-

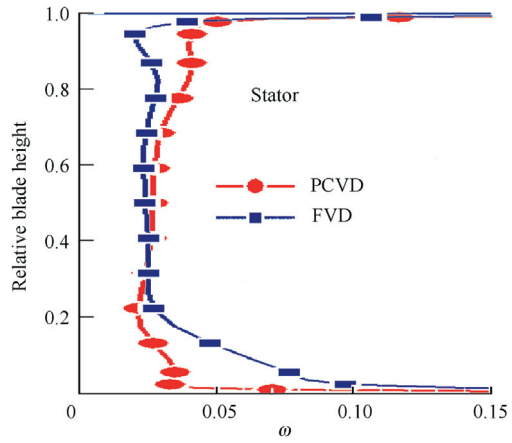

(a) Relative total pressure loss coefficients along the blade height of stator

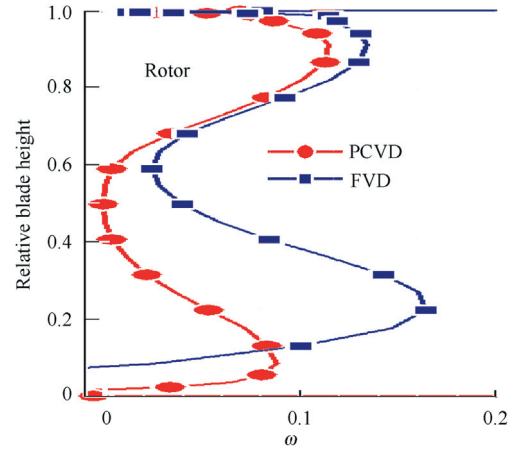

(b) Relative total pressure loss coefficients along the blade heightof rotor

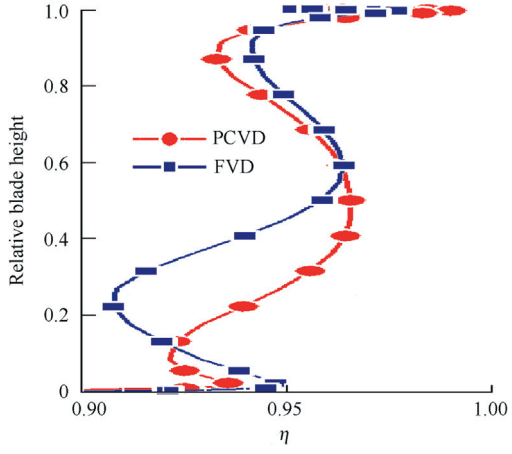

(c) Isentropic efficiency along the blade height

Fig. 13 Relative total pressure loss coefficients and isentropic efficiency along the blade height.

tion line on the SS. Thus the spanwise migration of hub endwall low-energy fluid along the SS is reduced. PCVD also results in a fall-off separation line on the SS and increases flow

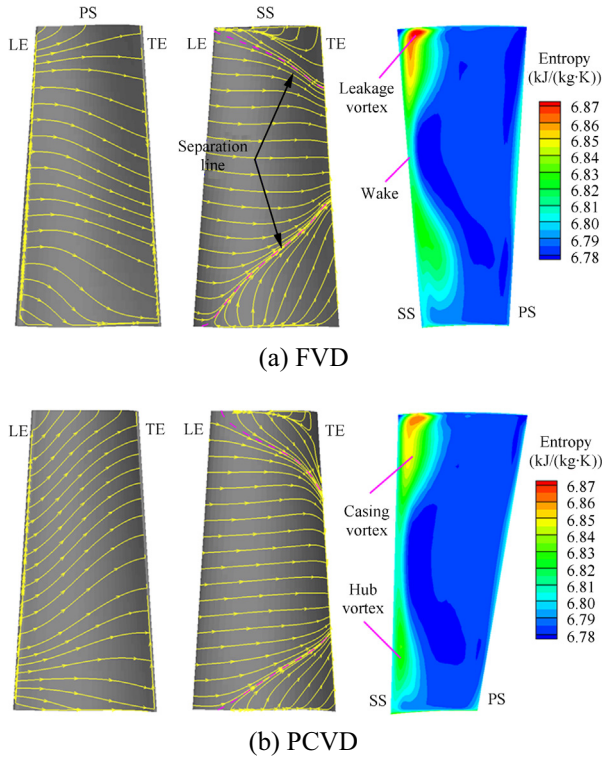

Fig. 14 Limiting streamlines on rotor blade surfaces and entropy distributions at the rotor exit.

migration along the span. All of these results can be inferred from the streamline oblique in the rear-tip corner region. Especially in the hub region, the typically outward boundary layer flow migration on the SS is minimized dramatically. This phenomenon cannot be explained by the transverse pressure gradient, since the pressure gradient from the PS to the SS does not decrease near the hub as mentioned in the preceding sections. In other words, the mildly outward flow migration is a result of competition between the counter-rotating PCVD-induced secondary vortex and the classical passage vortex. The calculations of static pressure distributions shown in Fig. 10 support this view. The streamlines on the PCVD rotor PS are inclined to migrate towards the rotor tip, indicating the tendency of PS boundary layer movement. While in FVD, the streamlines on the PS deflect towards the hub endwall. It is worth mentioning that due to the cross-passage endwall flow and the dominant centrifugal force in the blade passage, the flow field near the SS becomes very complicated. Therefore, the reverse movement of the boundary layer on the SS is not as obvious as that on PS.

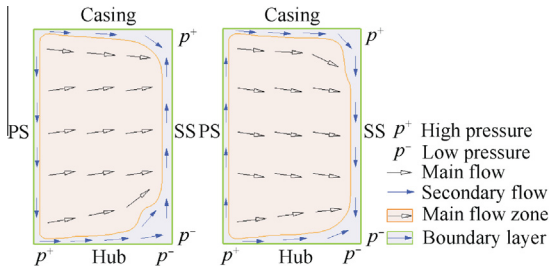

Fig. 15 Secondary flow structure in the traverse planes.

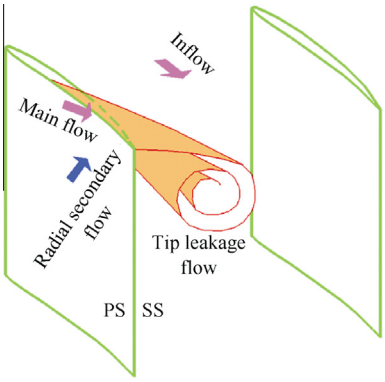

Fig. 16 Illustration of flow structure around the rotor tip.

The entropy distributions downstream from the rotor are also shown in Fig. 14. Two high-loss zones appear in the end-wall regions. Three distinct loss sources such as the tip leakage vortex, wake, and passage vortex are clearly seen in prediction. The separation phenomenon is controlled as indicated by its magnitude in the hub corner. The separation size reduction at the PCVD rotor hub leads to more flow passing the lower portion of the flow-path. PCVD also has a considerable influence on low-momentum fluid accumulation near the casing. The entropy generation of a tip high-loss region is less pronounced in PCVD, but its range is diffused over a large region and extended from the casing down to 60% span. In general, the PCVD blade restrains secondary flow near the hub and promotes it near the tip. The exit flow is more uniform for the PCVD stage on the whole.

Main flow features of secondary flow structure in the traverse planes can be summarized in Fig. 15. The PCVD blade is characterized by radially inward flow on the SS and radially outward flow on the PS, producing a novel spanwise migration on blade surfaces. This behavior can be accounted for not by the prevailing static pressure field but by the stream sheet twisting, because PCVD does not lead to a reverse pressure gradient (e.g., p^+, hub $> p^-$, tip) as evidenced from static pressure distributions in Fig. 10. As depicted in Fig. 15, the boundary layer migrates up to the PS, over the casing, and down to the SS, rotating in a direction opposite to that in FVD. The PCVD effect seems to produce a radial force to drive the main flow into the hub corner and the flow capacity in the hub corner is strengthened. Thus the anti-separation capacity becomes stronger and the separation in the hub corner is eliminated. This trend is just opposite above the mid-span, so the transverse motion gets stronger near the tip.

5.2.5. Influences on tip leakage flow

To help understand PCVD effect on the tip leakage flow, the flow structure inferred from CFD computations around the rotor tip is plotted in Fig. 16. It is obvious that a major component of the tip leakage flow vortex originates from the radial PS boundary layer migration. This radial boundary layer fluid has a very important influence on the tip leakage flow, producing a large blockage in the whole tip region. Less flow would be entrained into the gap due to the obstacle of this low-energy fluid. This radial secondary flow could be referred as the "blockage secondary flow". This part of low-momentum fluid is always underneath the tip leakage flow. As the radial secondary flow reenters the flow-path in the downstream side of the rotor, an additional mixing loss occurs.

The absolute value of the leakage massflow is 0.1176 kg/s, or 0.778% of the total massflow in PCVD, compared with 0.1647 kg/s, or 1.089% of the total massflow in FVD. This indicates a substantial reduction in the leakage flow through the gap due to PCVD.

6. Conclusions

(1) A single-stage turbine designed with the PCVD method demonstrates a 0.95% efficiency improvement compared to an equivalent FVD stage. The comparison results between flow solution and design data show a good agreement which demonstrates the superiority, feasibility, and validity of this method.
(2) The PCVD effects are actually obtained from the stream surface variation. Consequently an additional large-scale secondary vortex is induced which has a large impact on the qualitative pattern of the classical secondary flow. This method is very similar to the conventional CVD, except that the blade rows are designed to achieve specified radial distributions of axial velocity and static pressure.
(3) PCVD reveals a great ability of reducing tip clearance loss, relieving near-endwall secondary flow, and controlling high loss fluid radial migration. Although this article is focused on an axial turbine, most of research results are equally suitable for axial compressors and fans.
(4) The stage reaction of the PCVD turbine is greatly altered through biasing flow towards its rotor's inefficient hub sections. Although the turbine stage root reaction is increased, there is no increase in the axial thrust on the rotor.

Acknowledgement

The author would like to thank Fundamental Research Funds for the Central Universities (HEUCFZ1104) for funding this work.

References

1. Dorman TE, Welna H, Lindlauf RW. The application of controlled-vortex aerodynamics to advanced axial flow turbines. *J Eng Power* 1968;**90**(3):245–50.
2. Vad J, Bencze F, Corsini A, Rispoli F. Non-free vortex flow effects in an axial flow rotor. *Periodica Polytech Mech Eng* 2001;**45**(2):201–16.
3. Vad J, Bencze F, Benigni H, Glas W, Jaberg H. Comparative investigation on axial flow pump rotors of free vortex and non-free vortex design. *Periodica Polytech Mech Eng* 2002;**46**(2):107–16.
4. Bonaiuti D, Zangeneh M. On the coupling of inverse design and optimization techniques for turbomachinery blade design. In: *Proceedings of ASME Turbo Expo 2006: power for land, sea and air*; 2006.
5. Albuquerque RBF, Manzanares-Filho N, Oliveira W. Conceptual optimization of axial-flow hydraulic turbines with non-free vortex design. *Proc Inst Mech Eng A* 2007;**221**(5):713–25.

6. Szlivka F, Molnár I. Measured and non-free vortex design results of axial flow fans. *J Mech Sci Technol* 2008;**22**(10):1902–7.
7. Zheng Q, Gao J, Li B. Study of viscous controlled vortex design of a LP turbine stage. In: *Proceedings of ASME Turbo Expo 2010: power for land, sea and air*; 2010.
8. Sarraf C, Nouri H, Ravelet F, Bakir F. Experimental study of blade thickness effects on the overall and local performances of a controlled vortex designed axial-flow fan. *Exp Thermal Fluid Sci* 2011;**35**(4):684–93.
9. Deng QF, Zheng Q, Liu CL, Zhang H, Luo MC. Viscous controlled vortex design of a 1.5-stage axial subsonic test turbine. In: *Proceedings of ASME Turbo Expo 2011: power for land, sea and air*; 2011.
10. Friedrichs J, Baumgarten S, Kosyna G, Stark U. Effect of stator design on stator boundary layer flow in a highly loaded single-stage axial-flow low-speed compressor. In: *Proceedings of ASME Turbo Expo 2000*; 2000.
11. Gümmer V, Wenger U, Kau H-P. Using sweep and dihedral to control three-dimensional flow in transonic stators of axial compressors. *J Turbomach* 2001;**123**(1):40–8.
12. Zhao GJ, Chen F, Song YP, Wang ZQ. Experimental study on the aerodynamic performance of swept-curved blade. *Chin J Aeronaut* 2004;**17**(3):136–41.
13. Zhang YJ, Chen F, Feng GT, Su JX. Effect of turning angle on flow field performance of linear bowed stator in compressor at low Mach number. *Chin J Aeronaut* 2006;**19**(4):271–6.
14. Deng QF, Zheng Q, Liu CL, Li S. Pressure controlled vortex design of 15-stage turbine based on the method of controlling axial velocity variation. *Acta Aeronaut Astronaut Sin* 2011;**32**(11):2182–93 Chinese.
15. Stüer H, Truckenmüller F, Borthwick D, Denton JD. Aerodynamic concept for very large steam turbine last stages. In: *Proceedings of ASME Turbo Expo 2005: power for land, sea and air*; 2005.
16. Völker L, Casey M, Dunham J, Stüer H. The influence of lean and sweep in a low pressure steam turbine: throughflow modeling and experimental measurements. In: *Proceedings of ASME Turbo Expo 2008: power for land, sea and air*; 2008.

Deng Qingfeng received his B.S. and M.S. degrees from Harbin Engineering University (HEU) in 2006 and 2009, respectively. Now he is a Ph.D. candidate at HEU, majoring in aerothermodynamics and turbine design.

Zheng Qun is a professor at Harbin Engineering University. He received his Ph.D. degree in 2000. His main research fields are turbomachinery aerothermodynamics and computational fluid dynamics.